Journal of Fluorine Chemistry 168 (2014) 128–136

Contents lists available at ScienceDirect

Journal of Fluorine Chemistry

journal homepage: www.elsevier.com/locate/fluor

Self-assembled monolayers on gold generated from terminally perfluorinated alkanethiols bearing propyl vs. ethyl hydrocarbon spacers

Oussama Zenasni, Andrew C. Jamison, Maria D. Marquez, T. Randall Lee *

Departments of Chemistry and Chemical Engineering and the Texas Center for Superconductivity, University of Houston, Houston, TX 77204-5003, USA

ARTICLE INFO

Article history:
Received 19 May 2014
Received in revised form 26 August 2014
Accepted 2 September 2014
Available online 11 September 2014

Keywords:
Self-assembled monolayers
SAMs
Fluorinated alkanethiols
Fluorinated thin films
Conformational order
Packing density

ABSTRACT

This paper examines the structural and interfacial properties of terminally perfluorinated self-assembled monolayers (FSAMs) on gold generated from the adsorption of a new series of terminally perfluorinated propanethiols $F(CF_2)_n(CH_2)_3SH$, where $n = 8$, 10, and 12. Analysis of these FSAMs by ellipsometry and X-ray photoelectron spectroscopy (XPS) confirmed the formation of the monolayer films. The contact angles of water and *n*-hexadecane on these FSAMs indicated a high degree of hydrophobicity and oleophobicity. Polarization modulation infrared reflection-adsorption spectroscopy (PM-IRRAS) analysis of the films revealed that the fluorinated chains are oriented largely perpendicular to the gold surface. In addition, the FSAMs formed from the new adsorbates were compared to known FSAMs derived from $F(CF_2)_n(CH_2)_2SH$, where $n = 8$, 10, and 12, to examine the influence of the number of CH_2 groups in the short alkyl spacer upon the conformational order and packing structure of the films. Analysis of the XPS spectra for the normalized peak intensity of the F 1s and S 2p binding energies for both types of films suggest a *slight* increase in packing density for the chains having the propyl vs. the ethyl hydrocarbon spacer. This conclusion is consistent with the observed decrease in the wetting behavior of hexadecane on the FSAMs formed from the new adsorbates. However, the preponderance of the data indicates that these two series of partially fluorinated alkanethiols form films with highly similar structure/packing characteristics with no discernible "odd-even" effect between the two series.

1. Introduction

Fluorinated thin films serve as vital tools for modifying the surfaces of nanoscale devices. Such modifications include the adsorption of fluorinated amphiphiles on coinage metals as a means of corrosion prevention [1], on metal oxides to reduce stiction in microelectromechanical systems (MEMS) [2], and on medical implants as biomaterial coatings [3,4]. The motivation to use these adsorbates is tied to the ability of perfluorocarbon segments to transform the physical properties of an interface by influencing the wettability, friction, and barrier properties of the resulting surfaces [5–7]. Such modifications allow for the generation of films that exhibit low surface energy with coefficients of friction that are a quarter of that of polytetrafluoroethylene (PTFE) [8]. In addition, the fact that the molecules of these thin films are chemically bound to the surface offers an advantage over their polymeric counterparts when used as nanoscale boundary films to reduce friction.

One of the most widely explored classes of nanoscale boundary lubricants includes films known as self-assembled monolayers (SAMs), which are derived from the adsorption of either fluorinated or non-fluorinated adsorbate molecules, as illustrated in Scheme 1 [9–12]. In perhaps the most well known example, the adsorption of alkanethiols on Au(1 1 1) proceeds spontaneously with the sulfur headgroups binding covalently to the surface of the metal in a highly ordered array [9,12–15]. The alkyl spacer tilts to maximize interchain van der Waals (vdW) interactions, stabilizing the film. Normal alkanethiolate SAMs (HSAMs) formed on gold offer key advantages over other adsorbate/substrate combinations because of the inertness of gold as well as the moderately stable S–Au bond that enables the adsorbate molecules to migrate on the surface and maximize packing [9]. Both of these characteristics allow for precise control over the chemical and structural nature of the interface. This combination of features offers a more

* Corresponding author. Tel.: +1 713 743 2724; fax: +1 713 751 4445.
E-mail address: trlee@uh.edu (T.R. Lee).

http://dx.doi.org/10.1016/j.jfluchem.2014.09.003
0022-1139/

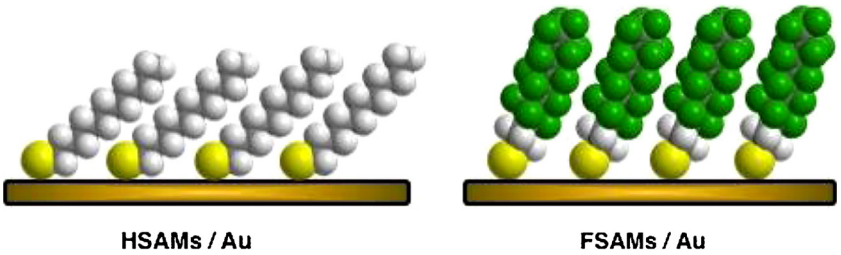

Scheme 1. Illustration of the differences in the tilt angle of thiolated chains in HSAMs as compared to FSAMs on gold.

comprehensive assessment of the effect of adsorbate chain modification on film properties as compared to other systems. Thus, concerning terminally perfluorinated adsorbates, the ability to control the number of fluorocarbon moieties in the tailgroup makes possible the production of fluorinated SAMs (FSAMs) with specific tunable properties [12,16].

SAMs generated from the adsorption of selectively fluorinated alkanethiols on gold have been used by many researchers as model thin films for evaluating the structural influences that determine the properties of these unique organic films [12,17,18]. Prior research has shown that the relatively large van der Waals diameter of the perfluorocarbon segments in FSAMs of the form $F(CF_2)_n(CH_2)_2SH$ (**FnH2**), where $n \geq 6$, causes the chains to be spaced ~5.7 Å apart, which is larger than that of normal HSAMs on gold (~4.9 Å) [19–21]. Such differences in chain spacing are partially attributable to the helical arrangement of the CF_2 units in the perfluorinated segments, as opposed to the *trans*-extended chain alignments adopted by CH_2 units in well-ordered *n*-alkanethiol-based monolayer films—an arrangement that maximizes the packing density of the chains [12]. Therefore, as illustrated in Scheme 1, FSAMs pack with their helical perfluorinated chains oriented roughly perpendicular to the surface, with a tilt angle ~11° from the surface normal, as opposed to well-packed HSAMs where the tilt angle is ~30° [22,23]. Such highly fluorinated thiolates form monolayers that adopt either a $c(7 \times 7)$ or $p(2 \times 2)$ hexagonal lattice, as compared to HSAMs with a $(\sqrt{3} \times \sqrt{3})R30$ hexagonal lattice [24,25].

The physical properties of such films are also directly affected by the size of the fluorocarbon segment [16,26–28]. Films of **FnH2** where $n = 8$ are poorly wettable by both water and oil [26]. This phenomenon can be attributed in part to the relatively large van der Waals radii of the perfluorinated segments, which has also been credited with influencing the effective interfacial energy (dispersive energy) for the exposed surface through a mechanism in which the packing density of the terminal CF_3 groups diminishes with increasing length of the perfluorinated segments [16]. Wettability studies of FSAMs generated from thiols of the form $F(CF_2)_n(CH_2)_mSH$ (**FnHm**, where the length of the fluorocarbon and hydrocarbon segments were varied, but the total chain length was held constant) vs. FSAMs generated from thiols of the form $F(CF_2)_n(CH_2)_{11}SH$ (**FnH11**, where the length of the fluorocarbon segment was varied but the hydrocarbon chain was held constant at eleven methylenes), indicated little additional influence from these extended fluorocarbon segments upon the measured contact angles with changes in the underlying SAM structure [16,27]. However, the interaction between a polar contacting liquid with each of the monolayers in the two series decreased with an increasing number of fluorocarbons until approximately $n = 5$. Previous studies have attributed this phenomenon to a burying of the dipole associated with the fluorocarbon–hydrocarbon (FC–HC) junction within the interface [16,28,29].

This report explores the structural and interfacial properties of FSAMs associated with a new class of highly fluorinated thiol-based adsorbates having a propyl group as an alkyl spacer and a relatively long fluorocarbon tailgroup: $F(CF_2)_n(CH_2)_3SH$; the **FnH3** series where $n = 8$, 10, and 12; **F8H3**, **F10H3**, and **F12H3**, respectively. These adsorbates are illustrated in Scheme 2 in the form of thiolates on gold. We compare the FSAMs formed from these new adsorbates to those formed from $F(CF_2)_n(CH_2)_3SH$; the **FnH2** series where $n = 8$, 10, and 12; **F8H2**, **F10H2**, and **F12H2**, respectively, whose characteristics have been extensively investigated [26,30]. Prior work on FSAMs formed from **FnH2** have shown that such adsorbates typically possess certain defects at the metal-thiol interface due to the spacing restrictions imposed by the larger vdW diameter of the fluorocarbon helix being so close to the substrate.

Thus, by extending the methylene spacer to three, we sought to evaluate the effect of such a change on the conformational order of the adsorbate chains as well as upon the interfacial properties of the resulting films. Further, we wished to examine whether these terminally fluorinated films would exhibit the

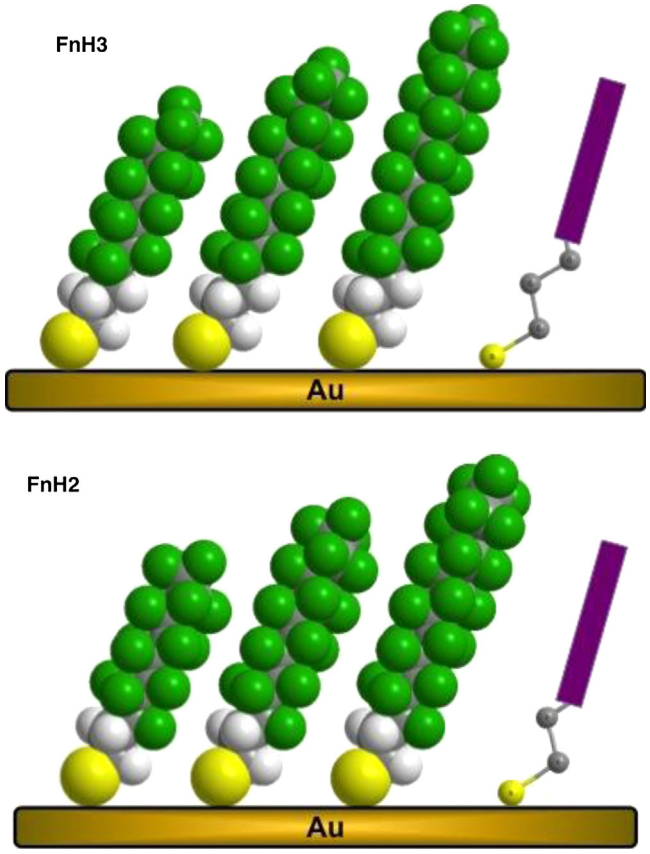

Scheme 2. Illustrations of the two series of adsorbates of the terminally perfluorinated FSAMs on gold that possess either three (**FnH3**) or two (**FnH2**) methylene spacers. The structural drawings on the right emphasize the presence of the alkyl segments between the surface bound headgroups and the rigid perfluorinated chains.

well known "odd-even" effects that are characteristic of highly ordered SAMs on gold, including those with CF_3-terminated hydrocarbon tailgroups [28,29,31]. Prior reports of thiolate SAMs with short alkyl spacers bearing rigid aromatic ring structures have pointed to a number of influences that might contribute to parity effects: the bending potential associated with the bonds of the headgroup to the substrate and to the alkyl spacer, the relative length of the alkyl spacer, and the rotation of the tailgroup around the bond with the alkyl spacer [32–35]. To explore the similarities and differences of the FSAMs in the present study, we characterized the films formed from both the **FnH3** series and the **FnH2** series using ellipsometry, contact angle goniometry, polarization modulation infrared reflection-adsorption spectroscopy (PM-IRRAS), and X-ray photoelectron spectroscopy (XPS). SAMs formed from octadecanethiol (**C18**) were used as reference standards for these studies.

2. Results and discussion

After successfully synthesizing the new adsorbates for the **FnH3** series, we tested their performance in forming terminally perfluorinated monolayer films on gold and compared these FSAMs to those of the **FnH2** series. We anticipated that the increase in the spacer length could offer better packing for the molecules, yet allow the fluorinated chains to still maintain their upright orientation with respect to the gold surface. To evaluate the FSAMs, we utilized XPS to analyze the atomic concentration on the gold surface and PM-IRRAS to determine the perfluoro-helix orientation for both classes of FSAMs examined. Furthermore, we measured the thicknesses and evaluated their wetting behavior to provide a complete set of data for determining the influence of the length of the short hydrocarbon spacer on the structure and interfacial properties.

2.1. Ellipsometric thicknesses of the films

Variation in the thickness of organic thin films is often detected utilizing ellipsometry, with numerous studies showing how this technique can be used to examine trends in thin film thickness for a homologous series of thiolate SAMs [15,36]. Therefore, we examined the two series of FSAMs by ellipsometry to determine if they produced similar trends and if the thickness values were consistent with the difference of a single methylene unit. As for the SAM formed from the adsorbate standard, **C18**, its thickness was compared to prior measurements collected on our ellipsometer, which gave an average thickness of 21 Å for data collected on seven samples over a one year timeframe. Table 4 shows the thicknesses of the **FnH3** series of FSAMs and the corresponding **FnH2** series, along with the data for the SAMs formed from **C18**. For the measurements taken utilizing a refractive index value of 1.45, a value typically used for alkanethiolate SAMs [26], the ellipsometric data indicate an increase in the thickness of the film going from **F8H3** (11 Å), to **F10H3** (13 Å), to **F12H3** (16 Å); an increment of ~1.2 Å per CF_2 unit. A similar trend is apparent in the data for the **FnH2** series: 10 Å, 12 Å, and 15 Å for $n = 8$, 10, and 12, respectively. Both sets of data align with prior published research, which reported a change of ~1.23 Å per CF_2 unit—a value associated with an average increase in the length of the perfluorinated segment for a homologous series of FSAMs [36]. When comparing the thicknesses of the **FnH3** series to that of the **FnH2** series, the data indicate that the **FnH3** thiols produce films that are ~1 Å thicker, a number that is in line with the increase in chain length by one methylene unit [36]. Additionally, we collected ellipsometric data using 1.33 as the refractive index—a value that has been used in prior studies of highly fluorinated thin films [26]. This second set of data is included in Table 1 for comparison, showing higher thicknesses, which is expected given the decrease in the value of the refractive index used in the calculation [26].

Table 1
Ellipsometric data for FSAMs formed from the **FnH3** and **FnH2** series as compared to the **C18** SAMs.

Adsorbate	1.45 Refractive index	1.33 Refractive index
F8H3	11	13
F10H3	13	16
F12H3	16	20
F8H2	10	13
F10H2	12	15
F12H2	15	19
C18	21	–

2.2. Analysis of the films using X-ray photoelectron spectroscopy

Analysis of the chemical composition of organic films by X-ray photoelectron spectroscopy not only provides an understanding of the elemental content of the monolayer, but also insight into the ordering of these systems. For the current study, the binding energy of the sulfur headgroup to the substrate was used as a reference point to determine the type of sulfur moieties present in the monolayer. All of the FSAMs of the **FnH3** series exhibited S 2p binding energies of 162.0 eV ($2p_{2/3}$) and 163.2 eV ($2p_{1/2}$), as shown in Fig. 1a, peak positions that have been assigned to thiolate sulfur species bound to gold [37,38]. Absent from these spectra are the characteristic peaks associated with sulfur, either as an unbound thiol or a disulfide (peaks typically found at 163.5–164.0 eV) [24,38,39] or in an oxidized state (generally located at ~168 eV) [40]. Therefore, analysis of the XPS spectra confirms the formation of the monolayers, the absence of any non-adsorbed species present in the film, and the integrity of these adsorbates upon the assembly of the FSAM.

The C 1s spectra for the **FnH3** FSAMs provided in Fig. 1b reveal three C 1s peak positions corresponding to the carbons of CF_3 at ~293.2 eV, CF_2 at ~290.8 eV, and CH_2 at ~284.8 eV, as shown in Table 2. Note that the intensity of the peaks corresponding to the CF_2 carbons increases in a manner proportional to the increase in the number of CF_2 units in the monolayer. This trend is also observed in the peaks corresponding to the F 1s binding energy, Fig. 1c, where the intensity of the peaks increase proportionally to the increasing number of fluorine atoms on the chain. Furthermore, these trends are also found in the XPS spectra for the FSAMs of the **FnH2** series, as shown in Table 2 and Fig. 2.

To evaluate the packing density of the **FnH3** FSAMs, we examined the ratio of the S 2p/Au 4f peak intensities for the **FnH3** FSAMs compared to the **FnH2** FSAMs [41]. Table 3 shows these data along with the composite peak intensity ratios for C 1s/Au 4f and F 1s/Au 4f for the **FnH3** and **FnH2** FSAMs. The ratios of the normalized sulfur peaks increase as the number of fluorocarbons increases: 0.93 for $n = 8$, 1.01 for $n = 10$, and 1.05 for $n = 12$, which indicates that the packing of the **FnH3** FSAMs with the longer perfluorinated segments is denser than that of the **FnH2** series, particularly in light of the increased attenuation of the sulfur signal on the **FnH3** series. To provide an alternative perspective on the surface packing, we also generated the C 1s/Au 4f ratios for the two series, which gave 1.07 for $n = 8$, 1.13 for $n = 10$, and 1.01 for $n = 12$. For these data, we anticipated values that reflected an additional carbon atom for the **FnH3** series. However, the value for the **F12H3** FSAM fails to align with the data obtained with the S 2p/Au 4f ratios. On the other hand, the depth and number of F 1s electrons is the same for a given length of fluorocarbon chain for two analogs (e.g., **F8H3** vs. **F8H2**). Therefore, changes in the

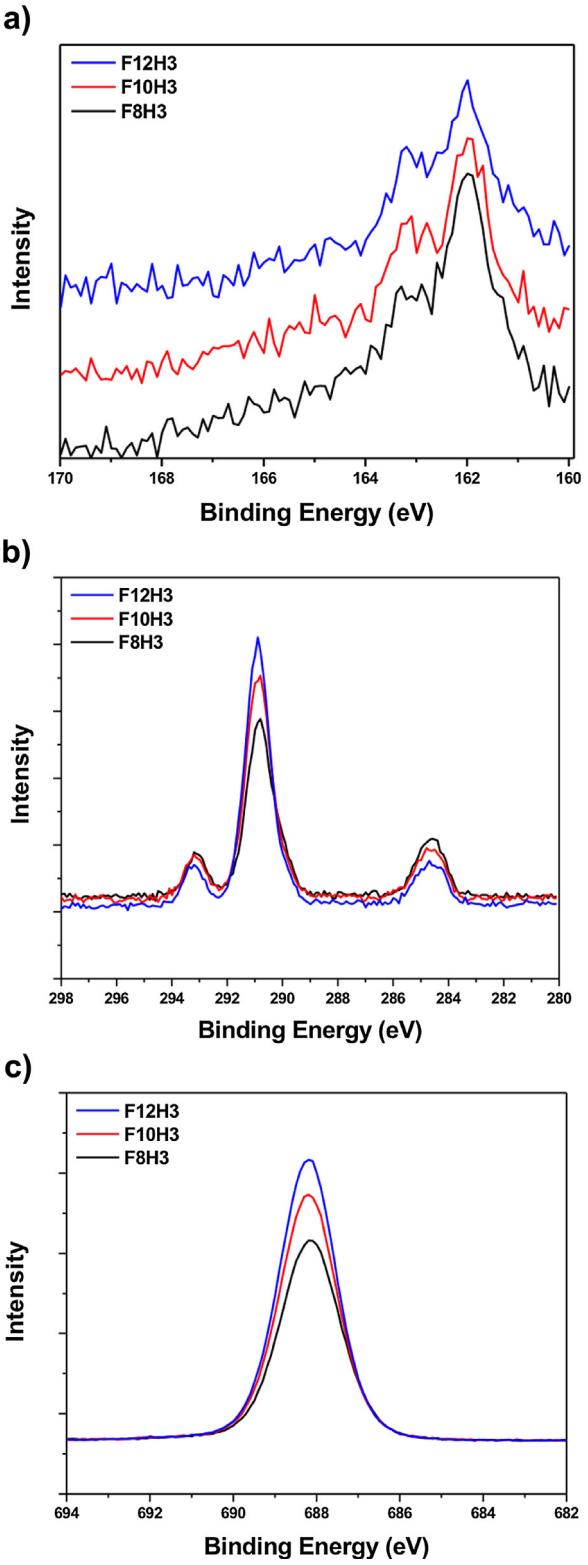

Fig. 1. XPS spectra for each of the FSAMs of the **FnH3** series: (a) the S 2p spectral region, (b) the C 1s spectral region, and (c) the F 1s spectral region.

normalized F 1s ratios per fluorocarbon chain size would better correlate to changes in the packing density of the perfluorinated helix as the number of methylenes increased from two to three. For our data (1.00 for $n = 8$, 1.05 for $n = 10$, and 1.01 for $n = 12$), the ratios indicate a slight improvement in packing associated with the longer propyl spacer.

Table 2
Peak positions for the **FnH3** and **FnH2** FSAMs for the XPS spectra displayed in Figs. 1 and 2.

Peak	**FnH3** (eV)			**FnH2** (eV)		
	$n = 8$	$n = 10$	$n = 12$	$n = 8$	$n = 10$	$n = 12$
C 1s (CF_3)	293.2	293.2	293.2	293.0	293.2	293.2
C 1s (CF_2)	290.8	290.8	290.9	290.7	290.9	291.0
C 1s (CH_2)	284.6	284.8	284.7	284.8	284.7	284.8
S $2p_{3/2}$	162.0	162.0	162.0	162.0	162.0	162.0
F 1s	688.2	688.2	688.2	688.1	688.2	688.2

Table 3
Ratios of the S 2p, C 1s, and F 1s XPS peak intensities for the **FnH3** FSAMs as compared to those of **FnH2**, using the peak intensity for Au 4f to normalize the values[a].

Fn	$(S\ 2p/Au\ 4f)_{FnH3}/(S\ 2p/Au\ 4f)_{FnH2}$	$(C\ 1s/Au\ 4f)_{FnH3}/(C\ 1s/Au\ 4f)_{FnH2}$	$(F\ 1s/Au\ 4f)_{FnH3}/(F\ 1s/Au\ 4f)_{FnH2}$
$n = 8$	0.93	1.07	1.00
$n = 10$	1.01	1.13	1.05
$n = 12$	1.05	1.01	1.01

[a] The ratios in this table were derived from the averages of two data sets.

2.3. Wettabilities of the films

For fluorinated thin films, the wettability of the surfaces have typically been probed with contacting liquids such as water (H_2O) and *n*-hexadecane (HD) to provide a measure of the interfacial hydrophobicity and oliophobicity, respectively. Furthermore, because contact angle measurements on SAMs are highly sensitive to small differences in the interfacial structure/composition of the films, additional insight into the nature of the packing and/or orientation of the adsorbates within the film can sometimes be gleaned from contact angle data. For FSAMs, the interpretation of the data can be complicated if the dipole arising from the fluorocarbon–hydrocarbon junction lies near the interface and influences the contact angles; however, for the current FSAMs, this dipole is sufficiently buried within the film that it should have no impact on the contact angles [16,28,29,42]. Assuming that the films expose perfluorinated surfaces of equivalent adsorbate density and surface ordering, the contact angle data should reveal only the influence of the fluorinated film, with a possible minor role from the underlying gold substrate [43].

The advancing contact angles (θ_a) of H_2O (a polar protic liquid) and HD (a nonpolar hydrocarbon liquid) measured on both series of FSAMs are shown in Table 4. FSAMs of the **FnH3** series and those of the **FnH2** series show the same high degree of hydrophobicity and oleophobicity, with contact angle values $\geq 115^\circ$ for H_2O and $\geq 73^\circ$ for HD. Note that all of the FSAMs are less wettable than the **C18** SAMs for both liquids, even though the latter is a well-packed film formed from the nanoscale equivalent of paraffin wax. For both series of films, the contact angles of water are generally equivalent for chains of equal perfluorocarbon length, but show a systematic increase in value with a lengthening of the perfluorocarbon segment (i.e., with increasing *n*). The effect of the monolayer thickness on wettability might reflect a reduction in the attractive van der Waals force between the contacting liquid and the underlying gold substrate as the thickness of the film increases (and the separation between them consequently increases) [43]. However, comparison of the contact angle data for the **FnH3** FSAMs vs. the **FnH2** FSAMs suggests that there is no strong influence from the underlying gold substrate, nor are there any "odd-even" effects in these contact angle data. The absence of such parity effects likely arise from the helical conformation of these perfluorinated termini and the low surface energy of

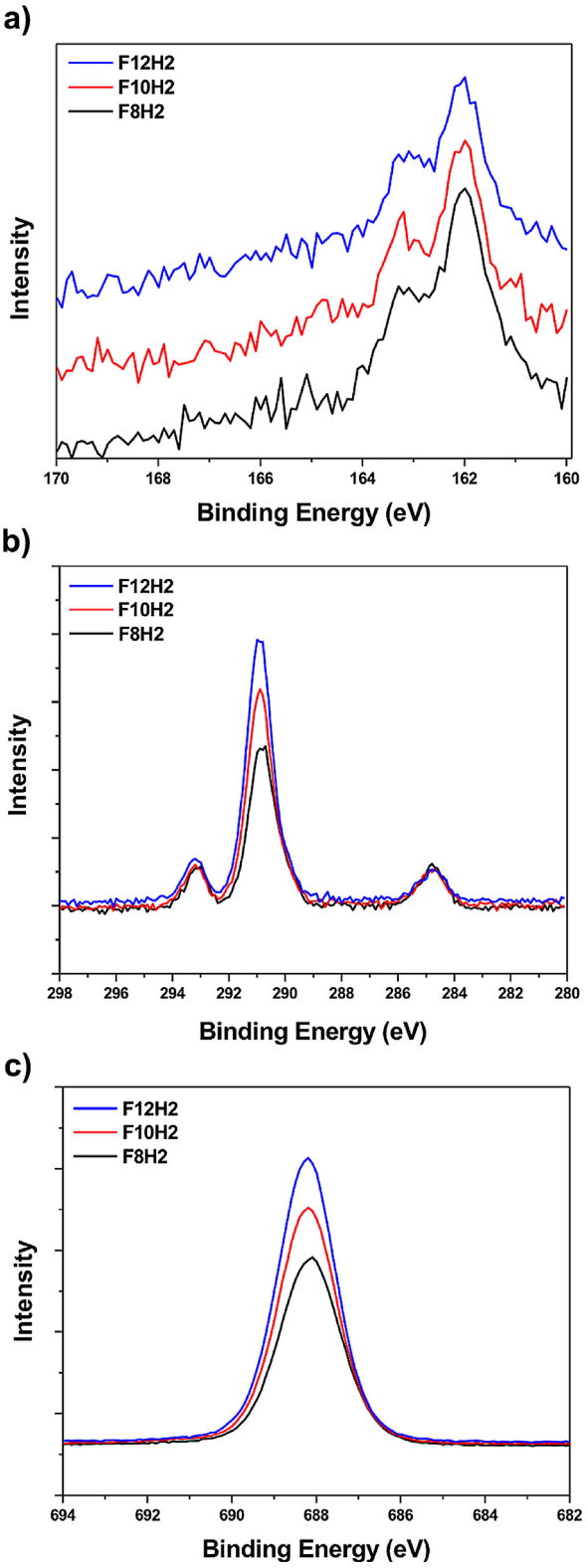

Fig. 2. XPS spectra for each of the FSAMs of the **FnH2** series: (a) the S 2p spectral region, (b) the C 1s spectral region, and (c) the F 1s spectral region.

fluorinated thin films formed from perfluorocarbon segments where $n \geq 6$ [16,42].

Similar conclusions can be drawn from the contact angle data for HD shown in Table 4. There are, however, slight indications that the **FnH3** FSAMs might be better organized than the **FnH2** FSAMs.

Table 4
Contact angles of FSAMs formed from the **FnH3** and **FnH2** series and the **C18** SAMs.

Adsorbate	H_2O (adv./rec.)	HD (adv./rec.)
F8H3	115/105	76/56
F10H3	116/106	76/60
F12H3	118/106	78/59
F8H2	115/104	73/56
F10H2	116/106	76/60
F12H2	117/106	77/60
C18	114/104	49/40

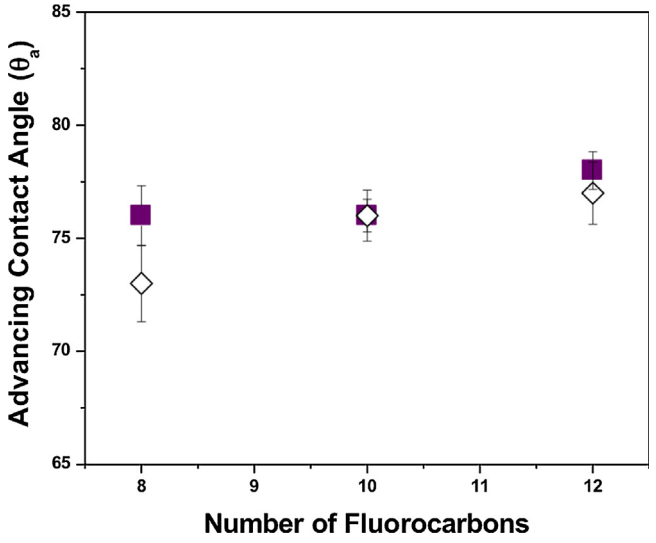

Fig. 3. Advancing contact angles (θ_a) for hexadecane on the **FnH3** (■) and **FnH2** (◇) monolayer films. (For interpretation of the references to color in this figure legend, the reader is referred to the web version of this article.)

In particular, the data in Table 4 and Fig. 3 show that the average value of θ_a for HD on **F8H3** (76°) is higher than that for **F8H2** (73°), which might be an indication that the FSAMs formed from the shortest perfluorocarbon chains benefit from an increase in distance between the relatively larger perfluorocarbon segments (as compared to the hydrocarbon segments) and the preferred lattice bonding sites on gold for thiols (vide supra). This difference is not evident in the F10 and F12 films from both series, perhaps because the interchain packing forces between the longer perfluorocarbon segments overcome the disorder introduced by having a short ethyl hydrocarbon spacer.

2.4. Analysis of the films using surface infrared spectroscopy

Surface IR spectra generally reveal information regarding SAM organization and orientation of the individual chains within the film. Due to the small number of methylene units in these chains, the C–H vibrational bands proved to be too weak to make reliable measurements, which limited our ability to use the collected PM-IRRAS data to determine the relative conformational order of the alkyl segments within these thin films, and also limited our insight into how the methylenes in the two systems might orient themselves to allow the overlying perfluorinated chain segments to afford similar exposed interfaces. However, analysis of the C–F stretching region in the PM-IRRAS spectra proved more fruitful. In Fig. 4, the bands between 1240 to 1280 and 1330 to 1380 cm^{-1}, designated as ν_{pd}^{CF2} (vibrational mode for CF_2 with a transition dipole perpendicular to the helical axis) and ν_{ax}^{CF2} (vibrational mode for CF_2 with a transition dipole parallel to the perfluorocarbon helical axis), respectively, provide evidence that *all* of the chains are oriented largely perpendicular to the surface for these

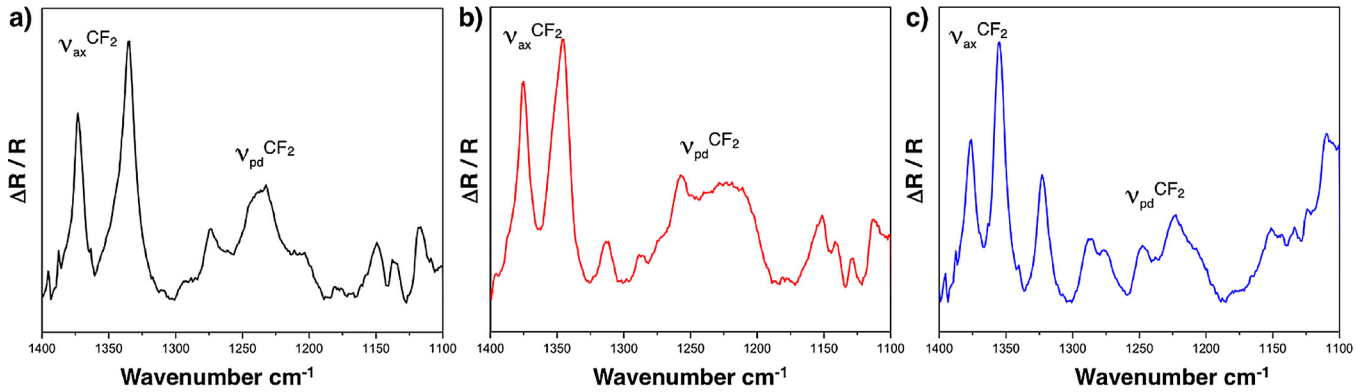

Fig. 4. PM-IRRAS spectra for the C–F stretching region of the films generated from the **FnH3** series: (a) **F8H3**, (b) **F10H3**, and (c) **F12H3**.

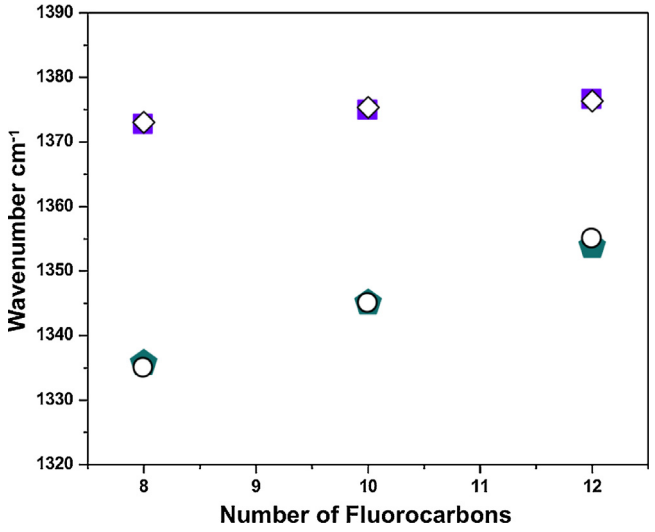

Fig. 5. Peak positions of the ν_{ax}^{CF2} bands as a function of fluorocarbon units in the FSAMs formed from the **FnH3** and **FnH2** series: first and second axial bands for **FnH3** series, (○) and (◇), respectively, and first and second axial bands for **FnH2** series, (⬟) and (■), respectively. (For interpretation of the references to color in this figure legend, the reader is referred to the web version of this article.)

FSAMs [27,44]. The data also suggest a slight decrease in the tilt of the chains as the size of the perfluorocarbon helix increases, based on the relative intensity of the two bands (ν_{ax}^{CF2} to ν_{pd}^{CF2}) for the spectra in Fig. 4. Previous studies have proposed that such a decrease in intensity of ν_{pd}^{CF2} compared to that ν_{ax}^{CF2} in the spectra of the surface IR is associated with a decrease in the tilt angle of the perfluorinated helix from the surface normal due to the orthogonal nature of the vibrational modes [27,44]. However, the exact tilt angle cannot be determined from this technique (from the as-is spectra) since we are unable to quantitatively compare the absolute intensities of a given vibration mode between spectra due to the signal modulation associated with the PM-IRRAS method [45–47].

Comparing the peak positions of the **FnH3** FSAMs to those of **FnH2**, the ν_{ax}^{CF2} bands appear at exactly the same wavenumber for a given perfluoroalkyl segment regardless of the number of underlying methylene units. As shown in Fig. 5, the peak positions of these bands shift with an increasing number of fluorocarbon units and appear to be specific to the size of the helix—a phenomena that has been noted previously [36].

3. Conclusions

A series of new terminally perfluorinated alkanethiols having short propyl hydrocarbon spacers were synthesized and used to generate self-assembled monolayers on gold. These new FSAMs were compared to those of known analogous FSAMs having short ethyl hydrocarbon spacers. Ellipsometric measurements confirmed the formation of monolayer films from all of the adsorbates and revealed that the **FnH3** FSAMs produced films that were consistently ~1 Å thicker than the **FnH2** FSAMs. Analysis by XPS provided additional support for a conclusion that FSAMs were successfully formed by showing that all of the sulfur atoms in the films were bound to the surface of gold. Analysis by XPS also revealed a slight increase in packing density at the gold surface for the **FnH3** FSAMs compared to the **FnH2** FSAMs. Contact angle measurements were further consistent with a model in which the propyl spacer allows for a slightly denser packing of the adsorbates on the surface of gold. The relative intensity of the ν_{pd}^{CF2} to ν_{ax}^{CF2} bands in the PM-IRRAS spectra indicated that the perfluorocarbon tailgroups were oriented largely perpendicular to the surface. In stark contrast to prior reports for thiolate SAMs bearing rigid aromatic tailgroups on short alkyl spacers, none of the data showed a discernible "odd-even" effect for **FnH3** FSAMs compared to **FnH2** FSAMs.

4. Materials and methods

4.1. Materials

Gold shot (99.999%) was purchased from Americana Precious Metals. Chromium rods (99.9%) were purchased from R. D. Mathis Company. Polished single-crystal silicon (1 0 0) wafers were purchased from Silicon Wafer Enterprises and rinsed with absolute ethanol (Aaper Alcohol and Chemical Co.) before use. *n*-Octadecanethiol (**C18**) was purchased from Sigma-Aldrich and used as received. The starting materials 1-iodo-1*H*,1*H*,2*H*,2*H*-perfluorodecane (94%), 1-iodo-1*H*,1*H*,2*H*,2*H*-perfluorododecane (94%), and 1-iodo-1*H*,1*H*,2*H*,2*H*-perfluorotetradecane (90%) were purchased from SynQuest Laboratory. Iodoperfluorooctane (98%), iodoperfluorodecane (98%), and iodoperfluorododecane (97%) were purchased from SynQuest Laboratory. Triethylamine (NEt_3), potassium thioacetate (KSAc), lithium aluminum hydride ($LiAlH_4$), allyl alcohol (99%), tributyltin hydride (Bu_3SnH), and methanesulfonyl chloride (MsCl) were purchased from Sigma-Aldrich Co. and used as purchased. Azobisisobutyronitrile (AIBN) was purchased from Sigma-Aldrich Co. and was recrystallized from methanol prior to use. Solvents used in the synthesis, 1,2-dichloroethane (DCE), tetrahydrofuran (THF), diethyl ether (Et_2O), toluene, and hexanes, were purchased from either Sigma-Aldrich or Avantor Performance Materials and used as received, unless stated otherwise. Magnesium sulfate ($MgSO_4$) was purchased from J. T. Baker Co., and sulfuric acid (H_2SO_4) was purchased from MACRON. Column chromatography was performed using silica gel (40–60 μm), and thin-layer

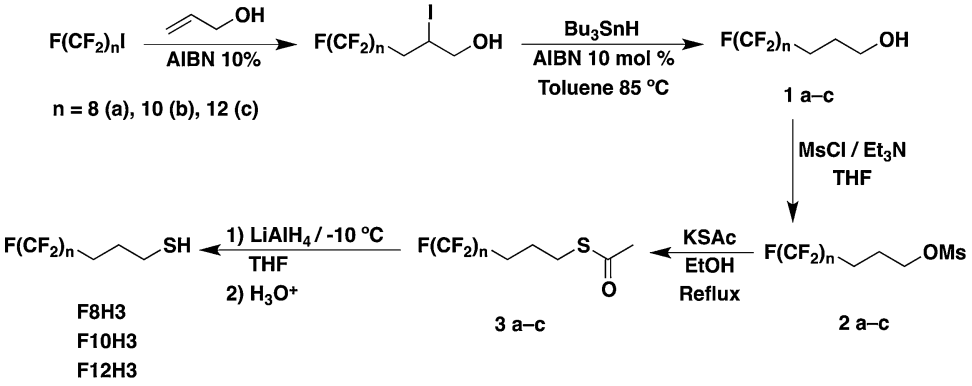

Scheme 3. Synthetic strategy used to prepare the fluorinated alkanethiol adsorbates of the form $F(CF_2)_n(CH_2)_3SH$, where n = 8, 10, and 12 (the **FnH3** series).

chromatography (TLC) was carried out using 200 μm-thick silica gel plates, both obtained from Sorbent Technologies, Inc. The developed TLC plates were visualized using molybdenum blue staining solution. Contacting liquids were of the highest purity available; *n*-hexadecane (HD) was purchased from Aldrich Chemical Co. and water was generated from a Milli-Q Water System with resistance of 18.2 MΩ (Millipore Corporation).

4.2. Synthesis of the adsorbates

4.2.1. Synthesis of terminally perfluorinated alkanethiols

The fluorinated alkanethiols having propyl hydrocarbon spacers were synthesized using the method illustrated in Scheme 3. The perfluorinated alkanethiols with spacers formed from two methylene units were synthesized according to a procedure found in the literature [30]. Because 1*H*,1*H*,2*H*,2*H*-perfluorotetradecanethiol has not been reported previously, its synthesis is also included in this subsection. Appendix A contains NMR spectra of the newly synthesized thiols.

4.2.2. Synthesis of the alcohol intermediates

In a 100-mL pear-shaped Schlenk flask, the starting 1-iodoperfluorooctane (5.00 g, 9.16 mmol), AIBN (10 mol%) and allyl alcohol (0.80 mL; ~12 mmol) were dissolved in DCE (30 mL). The system was degassed with three cycles of a standard freeze-pump thaw procedure. After warming to room temperature, the reaction mixture was heated to 85 °C for 8 h. The reaction was then cooled to room temperature, and an additional equivalent of AIBN was added under argon, followed by the same degassing method. The system was heated again to 85 °C for 8 h. The reaction percent conversion of perfluorinated iodide was monitored via ^{19}F NMR. The reaction was then transferred to a 250-mL round-bottom flask, and the solvent was removed by rotary evaporation. The crude product was dissolved in anhydrous toluene, and AIBN (10 mol%) was added. The reaction was heated to 60 °C and then Bu_3SnH (3.5 mL; 13 mmol) was added dropwise for 15 min. The reaction was then further heated to 85 °C and stirred at that temperature for 12 h. After removal of the volatiles, the crude product was dissolved in anhydrous Et_2O (200 mL). Excess of Bu_3SnH was removed under vacuum. Tributyltin iodide was converted to tributyltin fluoride by adding KF (1.246 g; 13.24 mmol), followed by stirring the resultant mixture at room temperature for 12 h. The mixture was filtered, and the solvent was removed by rotary evaporation. The crude product was carried to the next step without additional purification.

*4,4,5,5,6,6,7,7,8,8,9,9,10,10,11,11,11-Heptadecafluoroundecan-1-ol (***1a***).* ^1H NMR (400 MHz, $CDCl_3$): δ 3.74 (m, 2*H*, CH_2O), 2.21 (m, 2*H*, CH_2CF_2), 1.86 (m, 2*H*, CH_2CH_2).

*4,4,5,5,6,6,7,7,8,8,9,9,10,10,11,11,12,12,13,13,13-Henicosafluorotridecan-1-ol (***1b***).* This intermediate was prepared using a method analogous to that used to prepare intermediate **1a**. ^1H NMR (500 MHz, $CDCl_3$): δ 3.75 (q, J = 5.73 Hz, 2*H*, CH_2O), 2.22 (m, 2*H*, CH_2CF_2), 1.87 (m, 2*H*, CH_2CH_2).

*4,4,5,5,6,6,7,7,8,8,9,9,10,10,11,11,12,12,13,13,14,14,15,15,15-Pentacosafluoropenta-decan-1-ol (***1c***).* This intermediate was prepared using a method analogous to that used to prepare intermediate **1a**. ^1H NMR (500 MHz, $CDCl_3$): δ 3.75 (q, J = 5.54 Hz, 2*H*, CH_2O), 2.22 (m, 2*H*, CH_2CF_2), 1.87 (m, 2*H*, CH_2CH_2).

4.2.3. Synthesis of the mesylate intermediates

An aliquot of NEt_3 (4.4 mL; 32 mmol) was added to a solution of alcohol **1a** (5.00 g; 10.5 mmol) in anhydrous THF (50 mL) at room temperature while stirring. The resultant mixture was cooled to 0 °C under argon. After cooling, MsCl (8.1 mL; ~10 mmol) was added while stirring. The reaction was allowed to warm to room temperature and stirred for 6 h. The reaction was then quenched with ice-cold water (50 mL). The product was extracted with Et_2O (3 × 100 mL), and the combined organic phases were washed with 1 M aqueous HCl (1 × 100 mL), water (1 × 100 mL), and brine (1 × 100 mL). The organic layer was dried over anhydrous $MgSO_4$, followed by removal of the solvent by rotary evaporation to yield the crude product as a crystalline solid. Triturating these crystals in hexanes (50 mL) afforded the pure mesylate.

*4,4,5,5,6,6,7,7,8,8,9,9,10,10,11,11,11-Heptadecafluoroundecylmethanesulfonate (***2a***).* Obtained in 69% yield. ^1H NMR (500 MHz, $CDCl_3$): δ 4.32 (t, J = 6.02 Hz, 2*H*, CH_2O), 3.04 (s, 3*H*, CH_3), 2.25 (m, 2*H*, CH_2CF_2), 2.09 (m, 2*H*, CH_2CH_2).

*4,4,5,5,6,6,7,7,8,8,9,9,10,10,11,11,12,12,13,13,13-Henicosafluorotridecylmethanesulfonate (***2b***).* This intermediate was prepared using a method analogous to that used to prepare intermediate **2a**. Obtained in 80% yield. ^1H NMR (500 MHz, $CDCl_3$): δ 4.32 (t, J = 6.01 Hz, 2*H*, CH_2O), 3.04 (s, 3*H*, CH_3), 2.24 (m, 2*H*, CH_2CF_2), 2.09 (m, 2*H*, CH_2CH_2).

*4,4,5,5,6,6,7,7,8,8,9,9,10,10,11,11,12,12,13,13,14,14,15,15,15-Pentacosafluoropentadecyl-methanesulfonate (***2c***).* This intermediate was prepared using a method analogous to that used to prepare intermediate **2a**. Obtained in 78% yield. ^1H NMR (500 MHz, $CDCl_3$): δ 4.32 (t, J = 6.02 Hz, 2*H*, CH_2O), 3.04 (s, 3*H*, CH_3), 2.25 (m, 2*H*, CH_2CF_2), 2.08 (m, 2*H*, CH_2CH_2).

4.2.4. Synthesis of the thioacetate intermediates

In a three-necked round-bottom flask equipped with a condenser and an addition funnel, mesylate **2a** (1.0 g; 1.8 mmol) was dissolved in a blend of THF/ethanol (1:1) (100 mL) under argon. KSAc (0.616 g; 5.40 mmol) was dissolved in absolute ethanol (20 mL) (previously degassed), and added dropwise to the stirred mesylate solution under argon over 10 min. The

reaction was refluxed for 7 h. After the reaction was cooled to room temperature, water (100 mL) was added, and the resulting mixture was extracted with Et_2O (3 × 100 mL). The organic phases were combined and washed with water (1 × 100 mL), brine (1 × 100 mL), and then dried over $MgSO_4$. After evaporation of the solvent, the crude product was purified by column chromatography on silica gel (hexanes/DCE, 9/1).

*S-(4,4,5,5,6,6,7,7,8,8,9,9,10,10,11,11,11-Heptadecafluoroundecyl) ethanethioate (***3a***).* Obtained in 73% yield. ^{1}H NMR (500 MHz, $CDCl_3$): δ 2.95 (t, *J* = 7.16 Hz, 2*H*, CH_2S), 2.35 (s, 3*H*, $CH_3C(O)$), 2.16 (m, 2*H*, CH_2CF_2), 1.90 (m, 2*H*, CH_2CH_2).

*S-(4,4,5,5,6,6,7,7,8,8,9,9,10,10,11,11,12,12,13,13,13-Henicosafluorotridecyl) ethanethioate (***3b***).* This intermediate was prepared using a method analogous to that used to prepare intermediate **3a**. Obtained in 67% yield. ^{1}H NMR (500 MHz, $CDCl_3$): δ 2.95 (t, *J* = 7.16 Hz, 2*H*, CH_2S), 2.35 (s, 3*H*, $CH_3C(O)$), 2.14 (m, 2*H*, CH_2CF_2), 1.90 (m, 2*H*, CH_2CH_2).

*S-(4,4,5,5,6,6,7,7,8,8,9,9,10,10,11,11,12,12,13,13,14,14,15,15,15-Pentacosafluoropentadecyl) ethanethioate (***3c***).* This intermediate was prepared using a method analogous to that used to prepare intermediate **3a**. Obtained in 82% yield. ^{1}H NMR (500 MHz, $CDCl_3$): δ 2.95 (t, *J* = 7.16 Hz, 2*H*, CH_2S), 2.35 (s, 3*H*, $CH_3C(O)$), 2.14 (m, 2*H*, CH_2CF_2), 1.90 (m, 2*H*, CH_2CH_2).

4.2.5. Synthesis of the thiol final products

The perfluorothioacetate **3a** (0.5 g; 0.9 mmol) was dissolved in dry THF (50 mL) and added dropwise to a stirring slurry of $LiAlH_4$ (0.106 g; 2.80 mmol) in THF (10 mL) at 0 °C. The reaction was stirred at room temperature for 6 h under argon. The reaction was then quenched at 0 °C with water (25 mL, previously degassed), and was acidified with 1 M H_2SO_4 solution (previously degassed). The mixture was then extracted with Et_2O (3 × 100 mL). The combined organic phases were washed with water (1 × 100 mL) and brine (1 × 100 mL), dried over $MgSO_4$, filtered, and evaporated to dryness. The crude thiol product was purified by column chromatography on silica gel (hexanes).

*4,4,5,5,6,6,7,7,8,8,9,9,10,10,11,11,11-Heptadecafluoroundecane-1-thiol (***F8H3***)* was obtained as a colorless liquid in 73% yield. ^{1}H NMR (500 MHz, $CDCl_3$): δ 2.63 (q, *J* = 7.25 Hz, 2*H*, CH_2S), 2.23 (m, 2*H*, CH_2CF_2), 1.93 (m, 2*H*, CH_2CH_2), 1.38 (t, *J* = 8.02 Hz, 1*H*, *CH_2SH*); ^{19}F NMR (471 MHz, $CDCl_3$): δ-80.69 (3F, CF_3), −113.95 (2F, CF_2CH_2), −121.63 (2F, CF_2), −121.87 (4F), −122.65 (2F, CF_2), −123.37 (2F, CF_2), −126.05 (2F, CF_2); ^{13}C NMR (125 MHz, $CDCl_3$): δ 29.54 (t, J_{CF} = 22.04 Hz, C-3), 24.69 (s, C-2), 23.98 (s, C-1). Broad peaks at δ 108.19–120.38 are characteristic of a long perfluorocarbon chain [22]. GC–MS, *m*/*z*: 494 ($C_{11}H_7F_{17}SH^+$), 119 ($C_2F_5^+$), 69 (CF_3^+), 61 ($C_2H_5S^+$).

*4,4,5,5,6,6,7,7,8,8,9,9,10,10,11,11,12,12,13,13,13-Henicosafluorotridecane-1-thiol (***F10H3***)* was obtained as a white solid in 86% yield (mp: 66 °C). ^{1}H NMR (500 MHz, $CDCl_3$ at 40 °C): δ 2.62 (q, *J* = 7.22 Hz, 2*H*, CH_2S), 2.23 (m, 2*H*, CH_2CF_2): 1.93 (m, 2*H*, CH_2CH_2), 1.37 (t, *J* = 8.08 Hz, 1*H*, SH); ^{19}F NMR (471 MHz, $CDCl_3$ at 40 °C): δ-80.77 (3F, CF_3), −113.76 (2F, CF_2CH_2), −121.52 to −121.69 (10F), −122.54 (2F, CF_2), −123.29 (2F, CF_2), −125.95 (2F, CF_2); ^{13}C NMR (125 MHz, $CDCl_3$ at 40 °C): δ 29.63 (t, J_{CF} = 23.05 Hz, C-3), 24.70 (s, C-2), 23.89 (s, C-1). Broad peaks at δ 107.62–120.41 are characteristic of a long perfluorocarbon chain [22]. GC–MS, *m*/*z*: 594 ($C_{13}H_7F_{21}SH^+$), 119 ($C_2F_5^+$), 69 (CF_3^+), 61 ($C_2H_5S^+$).

*4,4,5,5,6,6,7,7,8,8,9,9,10,10,11,11,12,12,13,13,14,14,15,15,15-Pentacosafluoropenta-decane-1-thiol (***F12H3***)* was obtained as a white solid in 90% yield (mp: 101.6 °C). ^{1}H NMR (500 MHz, $CDCl_3$ at 40 °C): δ 2.62 (q, *J* = 7.22 Hz, 2*H*, CH_2S), 2.23 (m, 2*H*, CH_2CF_2), 1.92 (m, 2*H*, CH_2CH_2), 1.37 (t, *J* = 8.08 Hz, 1*H*, SH); ^{19}F NMR (471 MHz, $CDCl_3$): δ-80.62 (3F, CF_3), −113.92 (2F, CF_2CH_2), −121.60 to −121.76 (14F), −122.59 (2F, CF_2), −123.34 (2F, CF_2), −126.01 (2F, CF_2); ^{13}C NMR (125 MHz, $CDCl_3$ at 40 °C): δ 29.63 (t, J_{CF} = 22.25 Hz, C-3), 24.70 (s, C-2), 23.88 (s, C-1). Broad peaks at δ 108.64–120.41 are characteristic of a long perfluorocarbon chain [22]. GC-MS, *m*/*z*: 641 (M^+–HF–SH), 119 ($C_2F_5^+$), 69 (CF_3^+), 61 ($C_2H_5S^+$).

*1H,1H,2H,2H-perfluorotetradecanethiol (***F12H2***).* In a three-necked round-bottom flask equipped with a condenser and an addition funnel, 1-iodo-1*H*,1*H*,2*H*,2*H*-perfluorotetradecane (1.0 g, 1.3 mmol) was dissolved in a blend of THF/ethanol (2:1) (100 mL) under argon. An aliquot (0.29 g; 2.6 mmol) of KSAc was dissolved in absolute ethanol (20 mL) (previously degassed), and added to the stirred solution of starting material under argon over 10 min. The reaction was then refluxed for 7 h. After cooling, water (100 mL) was added to dissolve the potassium iodide salt. The mixture was extracted with Et_2O (3 × 100 mL), and the combined organic layers were washed with brine (1 × 100 mL), and then dried over $MgSO_4$. The solvent was removed by rotary evaporation, and the crude compound was dried under high vacuum for 12 h. The resulting crude thioacetate was dissolved in dried THF (50 mL) and added slowly to a stirred suspension of $LiAlH_4$ (0.10 g; ~2.6 mmol) in THF (10 mL) at 0 °C. The mixture was then stirred at room temperature for 10 h under argon, after which the reaction was quenched with water (25 mL) (previously degassed) at 0 °C and acidified with 1 M aqueous H_2SO_4 solution (25 mL) (previously degassed). The mixture was then extracted with Et_2O (3 × 100 mL), and the combined organic layers were washed with water (1 × 100 mL), brine (1 × 100 mL), dried over $MgSO_4$ and then filtered. The solvent was removed by rotary evaporation, and the crude product was purified by column chromatography on silica gel (hexanes) to give *1H,1H,2H,2H-perfluorotetradecanethiol* (**F12H2**) as a white solid in 68% yield from the starting iodide (mp: 103.5 °C). ^{1}H NMR (500 MHz, $CDCl_3$ at 50 °C): δ 2.79 (m, 2*H*, CH_2SH), 2.44 (m, 2*H*, CH_2CF_2), 1.61 (t, 1*H*, *J* = 8.25 Hz, SH); ^{19}F NMR (471 MHz, $CDCl_3$ at 50 °C): δ-80.72 (3F, CF_3), −113.95 (2F, CF_2CH_2), −121.37 to −121.55 (14F), −122.41 (2F, CF_2), −123.24 (2F, CF_2), −125.82 (2F, CF_2); ^{13}C NMR (125 MHz, $CDCl_3$ at 50 °C): δ 36.14 (t, J_{CF} = 22.25, C-2), 15.56 (s, C-1). Broad peaks at δ 107.62–120.41 are characteristic of a long perfluorocarbon chain [22].

4.3. Preparation of films

Gold substrates were prepared by thermal evaporation of the metals (chromium and then gold) onto Si(1 0 0) wafers under vacuum at a pressure $\leq 6 \times 10^{-5}$ Torr. The chromium layer of 100 Å was deposited on the silicon surface to aid in the adhesion of a subsequent 1000 Å layer of gold. To optimize film formation, the gold was deposited at a rate of 1 Å/s. The substrates were rinsed with absolute ethanol, dried with ultra-pure nitrogen gas, and used promptly after cleaning. Thiol solutions at 1 mM concentration in absolute ethanol were prepared in glass vials that had been previously cleaned with piranha solution and rinsed thoroughly with deionized water, followed by absolute ethanol. [*Caution: Piranha solution is highly corrosive, should never be stored, and should be handled with extreme care.*]. Two freshly cut and cleaned gold slides (3 cm × 1 cm) were inserted into each of the solutions. The thin film samples were allowed to equilibrate 48 h, after which they were rinsed with absolute ethanol and dried with ultra-pure nitrogen gas before characterization.

4.4. Characterization of SAMs

4.4.1. Ellipsometric thickness measurements

The thicknesses of the monolayers were measured using a Rudolph Research Auto EL III ellipsometer equipped with a He–Ne laser (632.8 nm). The incident angle was fixed at 70°. The refractive index (RI) of the sublayer was set to 1.45, in accordance with the established protocol [23]. Thickness measurements for the fluorinated films were also acquired with optical constants

determined using 1.33, an RI value associated with perfluorinated structures [26]. The calculated thickness value for each sample was the average of the data collected for measurements made at six points (i.e., three different points for each slide).

4.4.2. X-Ray photoelectron spectroscopy (XPS)

XPS spectra of the SAMs were obtained using a PHI 5700 X-ray photoelectron spectrometer with a monochromatic Al *K*α X-ray source ($h\nu$ = 1486.7 eV) incident at 90° relative to the axis of the hemispherical energy analyzer. Spectral data were collected using a takeoff angle of 45° from the surface and a pass energy of 23.5 eV. The binding energies were referenced to the Au $4f_{7/2}$ peak at 84.0 eV.

4.4.3. Wettability measurements

A ramé-hart model 100 contact angle goniometer was employed to measure the contact angles of water (H_2O) and *n*-hexadecane (HD) on the SAMs. The contacting liquids were dispensed (advancing contact angle, θ_a) and withdrawn (receding contact angle, θ_r) on the surface of the SAMs using a Matrix Technologies micro-Electrapette 25 at the slowest speed of 1 μL/s. The measurements were performed at room temperature (293 K) with the pipette tip in contact with the drop. The reported data for each sample were the average of measurements obtained from two slides working with three points per slide, collecting data at both edges of the drop.

4.4.4. Polarization modulation infrared reflection–absorption spectroscopy (PM-IRRAS)

Surface IR spectra were collected using a Nicolet Nexus 670 Fourier transform spectrometer equipped with a liquid-nitrogen-cooled mercury-cadmium-telluride (MCT) detector and a Hinds Instrument PEM-90 photoelastic modulator. The incident angle of the *p*-polarized light reflected from the sample was set to 80° with respect to the surface normal. The spectra of the C–F region were collected using 2048 scans at a spectral resolution of 4 cm^{-1}. The peak intensity for the spectra of the C–H stretching region was too weak to provide reliable data.

Acknowledgments

We are grateful for generous financial support from the Robert A. Welch Foundation (E-1320), the National Science Foundation (DMR-0906727), and the Texas Center for Superconductivity at the University of Houston.

Appendix A. Supplementary data

Supplementary data associated with this article can be found at http://dx.doi.org/10.1016/j.jfluchem.2014.09.003.

References

[1] T. Patois, T.A. Et, F. Lallemand, L. Carpentier, X. Roizard, J.-Y. Hihn, V. Bondeau-Patissier, Z. Mekhalif, Surf. Coat. Technol. 205 (2010) 2511–2517.
[2] U. Srinivasan, M.R. Houston, R.T. Howe, R. Maboudian, J. Microelectromech. Syst. 7 (1998) 252–260.
[3] R.L. Nicholson, M.L. Ladlow, D.R. Spring, Chem. Commun. (2007) 3906–3908.
[4] C.M. Santos, A. Kumar, W. Zhang, C. Cai, Chem. Commun. (2009) 2854–2856.
[5] E. Hoque, J.A. DeRose, P. Hoffmann, B. Bhushan, H.J. Mathieu, J. Chem. Phys. 126 (2007), 114706/114701-114706/114706.
[6] R.D. Weinstein, J. Moriarty, E. Cushnie, R. Colorado Jr., T.R. Lee, M. Patel, W.R. Alesi, G.K. Jennings, J. Phys. Chem. B 107 (2003) 11626–11632.
[7] H. Ma, H.-L. Yip, F. Huang, A.K.Y. Jen, Adv. Funct. Mater. 20 (2010) 1371–1388.
[8] S.P. Pujari, L. Scheres, T. Weidner, J.E. Baio, S.M.A. Cohen, R.C.J.M. van, H. Zuilhof, Langmuir 29 (2013) 4019–4031.
[9] A. Ulman, Chem. Rev. 96 (1996) 1533–1554.
[10] J.C. Love, L.A. Estroff, J.K. Kriebel, R.G. Nuzzo, G.M. Whitesides, Chem. Rev. 105 (2005) 1103–1169.
[11] C. Vericat, M.E. Vela, G. Benitez, P. Carro, R.C. Salvarezza, Chem. Soc. Rev. 39 (2010) 1805–1834.
[12] O. Zenasni, A.C. Jamison, T.R. Lee, Soft Matter 9 (2013) 6356–6370.
[13] A.C. Jamison, P. Chinwangso, T.R. Lee, in: W. Knoll, R.C. Advincula (Eds.), Functional Polymer Films, Wiley-VCH Verlag GmbH & Co., Weinheim, 2011, pp. 151–217.
[14] P. Chinwangso, A.C. Jamison, T.R. Lee, Acc. Chem. Res. 44 (2011) 511–519.
[15] A. Ulman, An Introduction to Ultrathin Organic Films, Academic, San Diego, CA, 1991.
[16] R. Colorado Jr., T.R. Lee, Langmuir 19 (2003) 3288–3296.
[17] F. Guittard, S. Geribaldi, J. Fluorine Chem. 107 (2001) 363–374.
[18] D. Barriet, T.R. Lee, Curr. Opin. Colloid Interface Sci. 8 (2003) 236–242.
[19] C.A. Alves, M.D. Porter, Langmuir 9 (1993) 3507–3512.
[20] S.N. Patole, C.J. Baddeley, D. O'Hagan, N.V. Richardson, F. Zerbetto, L.A. Zotti, G. Teobaldi, W.A. Hofer, J. Chem. Phys. 127 (2007), 024702/024701-024702/24702.
[21] H. Lu, D. Zeysing, M. Kind, A. Terfort, M. Zharnikov, J. Phys. Chem. C 117 (2013) 18967–18979.
[22] S. Frey, K. Heister, M. Zharnikov, M. Grunze, K. Tamada, R. Colorado Jr., M. Graupe, O.E. Shmakova, T.R. Lee, Isr. J. Chem. 40 (2000) 81–97.
[23] M.D. Porter, T.B. Bright, D.L. Allara, C.E.D. Chidsey, J. Am. Chem. Soc. 109 (1987) 3559–3568.
[24] K. Tamada, T. Ishida, W. Knoll, H. Fukushima, R. Colorado Jr., M. Graupe, O.E. Shmakova, T.R. Lee, Langmuir 17 (2001) 1913–1921.
[25] G.-y. Liu, P. Fenter, C.E.D. Chidsey, D.F. Ogletree, P. Eisenberger, M. Salmeron, J. Chem. Phys. 101 (1994) 4301–4306.
[26] C.E.D. Chidsey, D.N. Loiacono, Langmuir 6 (1990) 682–691.
[27] H. Fukushima, S. Seki, T. Nishikawa, H. Takiguchi, K. Tamada, K. Abe, R. Colorado, M. Graupe, O.E. Shmakova, T.R. Lee, J. Phys. Chem. B 104 (2000) 7417–7420.
[28] R. Colorado Jr., T.R. Lee, J. Phys. Org. Chem. 13 (2000) 796–807.
[29] M. Graupe, M. Takenaga, T. Koini, R. Colorado Jr., T.R. Lee, J. Am. Chem. Soc. 121 (1999) 3222–3223.
[30] C. Naud, P. Calas, H. Blancou, A. Commeyras, J. Fluorine Chem. 104 (2000) 173–183.
[31] F. Tao, S.L. Bernasek, Chem. Rev. 107 (2007) 1408–1453.
[32] F. Chesneau, B. Schupbach, K. Szelagowska-Kunstman, N. Ballav, P. Cyganik, A. Terfort, M. Zharnikov, Phys. Chem. Chem. Phys. 12 (2010) 12123–12137.
[33] J. Dauselt, J. Zhao, M. Kind, R. Binder, A. Bashir, A. Terfort, M. Zharnikov, J. Phys. Chem. C 115 (2011) 2841–2854.
[34] A. Shaporenko, M. Brunnbauer, A. Terfort, M. Grunze, M. Zharnikov, J. Phys. Chem. B 108 (2004) 14462–14469.
[35] H.-T. Rong, S. Frey, Y.-J. Yang, M. Zharnikov, M. Buck, M. Wuehn, C. Woell, G. Helmchen, Langmuir 17 (2001) 1582–1593.
[36] R. Colorado Jr., M. Graupe, O.E. Shmakova, R.J. Villazana, T.R. Lee, in: J.E. Frommer, R. Overney (Eds.), Interfacial Properties on the Submicron Scale, American Chemical Society, Washington, DC, 2001, pp. 276–292.
[37] A.C. Jamison, S. Zhang, O. Zenasni, D.K. Schwartz, T.R. Lee, Langmuir 28 (2012) 16834–16844.
[38] L.O. Srisombat, S. Zhang, T.R. Lee, Langmuir 26 (2010) 41–46.
[39] D.G. Castner, K. Hinds, D.W. Grainger, Langmuir 12 (1996) 5083–5086.
[40] B. Singhana, S. Rittikulsittichai, T.R. Lee, Langmuir 29 (2013) 561–569.
[41] J.-S. Park, A.N. Vo, D. Barriet, Y.-S. Shon, T.R. Lee, Langmuir 21 (2005) 2902–2911.
[42] M. Takenaga, S. Jo, M. Graupe, T.R. Lee, J. Colloid Interface Sci. 320 (2008) 264–267.
[43] W.J. Miller, N.L. Abbott, Langmuir 13 (1997) 7106–7114.
[44] T.J. Lenk, V.M. Hallmark, C.L. Hoffmann, J.F. Rabolt, D.G. Castner, C. Erdelen, H. Ringsdorf, Langmuir 10 (1994) 4610–4617.
[45] T. Buffeteau, B. Desbat, J.M. Turlet, Appl. Spectrosc. 45 (1991) 380–389.
[46] T. Buffeteau, B. Desbat, D. Blaudez, J.M. Turlet, Appl. Spectrosc. 54 (2000) 1646–1650.
[47] M.A. Ramin, G. Le Bourdon, N. Daugey, B. Bennetau, L. Vellutini, T. Buffeteau, Langmuir 27 (2011) 6076–6084.